Martin Veidt and Ching-Tai Ng
Influence of stacking sequence on scattering characteristics of the fundamental anti-symmetric Lamb wave at through holes in composite laminates
Journal of the Acoustical Society of America, 2011; 129(3):1280-1287

Influence of stacking sequence on scattering characteristics of the fundamental anti-symmetric Lamb wave at through holes in composite laminates

Martin Veidt and Ching-Tai Ng [a)]

School of Mechanical and Mining Engineering, The University of Queensland, Brisbane, Qld, 4072, Australia

Submission of Original Manuscript: April 7, 2010

Submission of Revised Manuscript: August 31, 2010

[a)] Author to whom correspondence should be addressed. Electronic mail: uqcng2@uq.edu.au

Abstract

This paper investigates the scattering characteristics of the fundamental antisymmetric (A_0) Lamb wave at through holes in composite laminates. Three-dimensional (3D) finite element (FE) simulations and experimental measurements are used to study the physical phenomenon. Unidirectional, bidirectional and quasi-isotropic composite laminates are considered in the study. The influence of different hole diameter to wavelength aspect ratios and different stacking sequences on wave scattering characteristics are investigated. The results show that amplitudes and directivity distribution of the scattered Lamb wave depend on these parameters. In the case of quasi-isotropic composite laminates, the scattering directivity patterns are dominated by the fiber orientation of the outer layers and are quite different for composite laminates with the same number of laminae but different stacking sequence. The study provides improved physical insight into the scattering phenomena at through holes in composite laminates, which is essential to develop, validate and optimize guided wave damage detection and characterization techniques.

PACS numbers: 43.35.Cg, 43.35.Zc

I. INTRODUCTION

The application of Lamb waves, often called guided waves, has been established as the method of choice for quantitative nondestructive evaluation and structural health monitoring for plate like structures[1-3]. Guided wave techniques have successfully been used to detect fatigue cracks and corrosion damage in metals, debonds in bonded joints and delaminations in composite laminates[4-7]. The understanding of the scattering characteristics of guided waves at these damages and at structural features where these damages frequently initiate, in particular fastener holes, is an essential requirement to enable the development and optimization of quantitative damage detection and characterization methodologies for complex engineered structures.

For isotropic materials, different analytical models have been developed to predict the Lamb waves scattering at cylindrical inhomogeneities. Vemula and Norris[8] and McKeon and Hinders[9] presented an analytical solution for anti-symmetric (A_0) and symmetric (S_0) Lamb waves scattering at cylindrical defects in isotropic plate based on the Mindlin plate theory, respectively. Fromme and Sayir[10] experimentally validated the A_0 Lamb wave scattering by a through hole using classical and Mindlin plate theory. Cegla *et al.*[11] presented an analytical solution for Lamb wave scattering from a non-symmetric blind hole in isotropic plates using Poisson and Mindlin plate theories. Mode conversion from S_0 to A_0 Lamb wave was considered in the study and the model was validated using experimental measurements. Moreau and Castaings[12] proposed an orthogonality relation to reduce the size of the FE models for the simulation of scattering problems of three-dimensional (3D) Lamb waves in isotropic material. Only a small number of previous 3D analyses are available for composite laminates, especially in the context of the scattering of guided waves at defects or structural features such as fastener holes[12,13]. Recently, Ng and Veidt[14] presented a comprehensive 3D finite element (FE) and experimental study of A_0 Lamb wave scattering at a delamination in composite laminates.

This paper investigates A_0 Lamb wave scattering at a through hole with a particular

focus on the influence of the laminate stacking sequence on the scattering characteristics. The reason to focus on A_0 Lamb wave is its shorter wavelength compared to corresponding S_0 Lamb wave at the same frequency. This makes it potentially more sensitive to small damage, which is particularly important for damage initiating at fastener holes. In addition A_0 Lamb waves are generally easier activated and have larger signal magnitudes than S_0 Lamb waves at low frequency. Due to these advantageous characteristics, the use of A_0 Lamb waves has recently attracted considerable interest in quantitative damage evaluation[7,15,16].

The paper starts by describing the 3D FE simulations and experimental setup for obtaining the scattered Lamb waves at a through hole in a composite laminate in Section II. The results of the experimental validation of the FE simulations are presented in Section III. The validated FE model is then used in Sections IV and V to investigate the influence of hole diameter to wavelength aspect ratio and laminate stacking sequence on the wave scattering characteristics. Finally, conclusions are presented in Section VI.

II. THREE-DIMENSIONAL FINITE ELEMENT SIMULATIONS

3D FE method is employed to simulate the Lamb waves propagation and scattering at a through hole of composite laminates. The program ANSYS[17] was used to generate the geometry and perform the meshing of the model. The numerical simulations were then solved by explicit FE code LS-DYNA[18]. Composite laminates consisting of 8-ply Cycom® 970/T300 unidirectional carbon/epoxy prepreg lamina but with different stacking sequences are considered in this study. The fiber volume fraction and density of each lamina are 0.55 and 1517 kg/m^3, respectively. The effective material properties were determined by micromechanical modeling[19] and are given in Table I. The dimension of the FE models is 180×180×1.6 mm^3. A circular through hole located at the centre of the laminate is created by removing FE elements. Each lamina was modeled using eight-noded 3D reduced integration solid brick elements with hourglass control. Each node of the solid brick element has three degrees-of-freedom (DoF). A small stiffness-weighted damping was considered to enhance

the numerical stability and simulate the damping effect of the composite material. The A_0 Lamb wave is excited by applying out-of-plane nodal displacement to the surface nodes covered by a half circle (5 mm diameter) transducer area (as shown in Fig. 1). The transducer is located 90 mm away from the centre of the through hole. The excitation signal is a 140 kHz narrow-band six-cycle sinusoidal tone bust pulse modulated by a Hanning window. The A_0 Lamb wave signals at particular locations are obtained by monitoring the out-of-plane nodal displacement of the nodes located at the mid-thickness of the laminate. This ensures that only the A_0 Lamb mode is detected as the S_0 and SH_0 Lamb modes have zero out-of-plane displacement at the mid-thickness location. Composite laminates with different stacking sequences are considered in this paper. The theoretically calculated wavelengths at zero degree direction are between 7.1 to 9.8 mm depending on the stacking sequence of the laminates. A summary is given in Table II. A very fine mesh is used for the whole model in which the elements have in-plane square shape with dimensions 0.4×0.4 mm^2, which guarantees that more than seventeen nodes exist per wavelength in any propagation direction in any composite laminate which is substantially more than the minimum requirement of ten nodes stated in the literature[7,20,21]. The thickness of each solid element is 0.2 mm which results in an aspect ratio of two for the solid elements. A convergence study confirmed that simulation results using elements with aspect ratio two have the identical accuracy compared to cubic elements. The total number of solid brick elements is approximately 1.62 million and the models have in the order of 10 million DoF and require around six hours to solve. The time step is automatically controlled by ANSYS/LS-DYNA depending on the smallest element size. It is approximately 20 ns, which is sufficient to capture any A_0 as well as S_0 Lamb wave propagation.The hourglass energy was guaranteed less than 2% of the internal energy for all simulations which ensures the accurate prediction of the scattered Lamb waves[22].. Fig. 2 shows typical time snapshots of the FE simulated out-of-plane displacement for a $[45/-45/0/90]_S$ quasi-isotropic composite laminate. Fig. 2a shows the A_0 Lamb wave soon after excitation. Fig. 2b shows the scattering of the Lamb wave at a through hole. The scattered Lamb waves generated at the hole is clearly visible.

A. Scattered Lamb waves extraction

By carrying out two simulations with the same meshing for the identical laminate with and without hole, the scattered wave generated from the interaction of the incident wave with the hole can be extracted and completely separated from the incident waves by

$$u_{r,\theta}^{(S)}(t) = u_{r,\theta}^{(D)}(t) - u_{r,\theta}^{(U)}(t) \tag{1}$$

where $u_{r,\theta}^{(D)}(t)$ and $u_{r,\theta}^{(U)}(t)$ are the numerically calculated out-of-plane displacement components of Lamb waves at location (r,θ) for the laminate with and without hole, respectively. $u_{r,\theta}^{(S)}(t)$ is the out-of-plane displacement components of extracted scattered Lamb waves from a through hole. r and θ are the radial and azimuthal coordinates of the cylindrical coordinate system shown in Fig. 1.

For determining the scattering directivity pattern (SDP), the out-of-plane displacement of 36 nodal points at r = 40 mm and $0° \le \theta \le 360°$ with 10° step increments are calculated for both intact and damaged composite laminates. As the monitoring locations are many incident wavelengths away from the excitation, the generated evanescent waves are not present in the received signal. The SDP of the Lamb waves is obtained by determining the maximum absolute amplitude of the calculated scattered Lamb waves using Equation (1) in time domain. Each plot of the SDP is normalized by the maximum absolute amplitude of the incident Lamb wave at the through hole centre location of the intact composite laminate.

III. EXPERIMENTAL VALIDATION

A. Experimental setup

A $[45/-45/0/90]_S$ quasi-isotropic composite laminate manufactured from eight layers of Cycom® 970/T300 unidirectional carbon/epoxy prepreg lamina (as shown in Table I) was used to validate the results from FE simulations. The dimension of the composite laminate is

600×600×1.6 mm^3. A piezoceramic disc (Ferroperm Pz27) with 5 mm diameter and 2 mm thickness was adhesively bonded to the composite laminate to excite the A_0 Lamb wave. The piezoceramic disc was located at r = 90 mm and θ = 180°. The excitation signal is a 140 kHz narrow-band six-cycle sinusoidal tone bust pulse modulated by a Hanning window which is identical to the numerical simulation. The excitation signal is generated by a computer controlled arbitrary waveform generator (Stanford Research DS345) with 10 V peak-to-peak output voltage. A power amplifier (Krohn Hite model 7500) was used to amplify the excitation signal by a factor of 10-50 before it was applied across the electrodes of the piezoceramic transducer. The out-of-plane displacements were measured by a laser Doppler vibrometer (OFV 303/OFV 3001, Polytech GmbH) and a thin reflective tape was attached to the surface of the laminate to enhance the optical backscatter laser beam. The laser head was positioned by a computer controlled positioning system (Newport ESP 300). The measured out-of-plane displacement was then captured by a Tektronix TDS420A oscilloscope and transferred to a PC for analysis. The setup is shown in Fig. 3. The quality of each measurement was improved by applying a bandpass filter and averaging the signals over 1000 acquisitions. The scattered wave from the through hole was extracted using the method described in Section II.A. It should be noted that the material properties of composite laminates, the size of the transducer, the location of the transducer and the measurement relative to the center of the through hole are identical to the numerical simulations to ensure a direct comparison between the results from the numerical simulations and the experimental measurements.

B. Propagation of Lamb waves

The FE simulated Lamb waves were first validated by the experimental measurements to ensure the accuracy of the simulation results. Fig. 4a shows the normalized out-of-plane amplitude of the incident Lamb wave at $r = 40$ mm and $\theta = 0°$. It can be seen that there is an excellent agreement between the simulated and experimentally measured incident A_0

Lamb wave. Fig. 4b shows the comparison of the group velocity dispersion curves between the theoretical, FE simulation and experimental results for $\theta = 0°$. The theoretical results are obtained by using the program DISPERSE[23] and is indicated by solid lines. The circles and triangles represent FE simulation and experimental results, respectively. The curves were obtained by sweeping the excitation frequency from 20 to 300 kHz in steps of 20 kHz.

The group velocity of each excitation frequency is estimated from the energy density spectrum of the measured out-of-plane displacement which is calculated by using the continuous Gabor wavelet transform[24,25]. By convolving the measured out-of-plane displacement $u(t)$ with the translation p and dilation q, the continuous wavelet transform coefficient $WT(p,q)$ can be obtained as

$$WT(p,q) = \int_{-\infty}^{\infty} u(t)\psi_{p,q}^{*}(t)\,dt \tag{2}$$

where

$$\psi_{p,q}(t) = \frac{1}{\sqrt{q}}\psi\left(\frac{t-p}{q}\right) \tag{3}$$

The asterisk denotes the complex conjugate and $\psi(t)$ is the mother wavelet which is chosen to be the Gabor function defined as

$$\psi(t) = \frac{1}{\sqrt[4]{\pi}}\sqrt{\frac{\omega_0}{\lambda}}\exp\left[-\frac{(\omega_0/\lambda)^2}{2}t^2 + i\omega_0 t\right] \tag{4}$$

The values of ω_0 and λ influence the resolution in the time-frequency analysis and are usually chosen as 2π and $\pi\sqrt{2/\ln 2} \approx 5.336$, respectively[24]. The energy density spectrum is calculated as $|WT(p,q)|^2$. It indicates the energy distribution of the measured signal $u(t)$ around $t = p$ and $\omega = \omega_0/q$ which provides an accurate and powerful tool for evaluating the arrival time of Lamb waves at the excitation frequency. As shown in Fig. 4b, excellent agreement is found between the theoretical, FE simulation and experimental results.

Fig. 4c compares the decay of the numerically simulated and experimentally measured incident Lamb wave for 10 mm $\leq r \leq$ 150 mm and $\theta = 0°$. The measurement was carried out at three different locations to detect possible spatial dependence of the composite laminate. The out-of-plane amplitude is normalized by the amplitude measured at r = 10 mm to enable comparison between the numerically simulated and experimentally measured results. The figure shows that the three measurements at the same distance away from the excitation centre are slightly different to each other but the variation is minimal indicating the good quality of the manufacturing process. The numerical simulation gives an excellent prediction of the amplitude decay of the Lamb waves.

Fig. 5 shows a polar directivity plot of the maximum absolute incident Lamb wave amplitude at r = 40 mm and $0° \leq \theta \leq 360°$ with 10° step increment. The amplitude at each direction was normalized by the mean of the maximum absolute amplitudes of all directions. This leads to a direct comparison of the results between the numerical simulation and experimental results. Very good agreement is found between the numerical simulations and experimental results. It should be noted that although the angular distribution of phase and group velocity for quasi-isotropic composite laminates are almost isotropic for A_0 Lamb wave[26], the angular distribution of the wave amplitude is anisotropic. This indicates that the energy flow of the Lamb waves is influenced by the stacking sequence of the composite laminate[27,28]. The scattering energy is mainly focused around $\theta = 45°$ and -45° indicating that the energy flow of the A_0 Lamb wave tends to be focused along the fiber directions of the outer laminae.

C. Scattering directivity pattern

The previous section demonstrated that the FE simulation is able to accurately predict the Lamb wave propagation characteristics in composite laminates. This section validates the FE simulation for Lamb wave scattering at through holes for three different hole sizes (3 mm, 5 mm and 8 mm diameter). The corresponding through hole diameter (d) to wavelength (λ)

ratios ($R_{TW} = d/\lambda$) at $\theta = 0°$ are 0.38, 0.63 and 1.01. The through holes were generated by using solid carbide 8-facet special purpose drills for composite laminate machining. Fig. 6 shows a comparison of the SPD between the FE simulated and experimental measured data. It can be seen that there is very good agreement between the FE and experimental results. This shows that the FE simulation is able to accurately predict the SDP of a through hole. It can be seen that backward scattering is dominating for small R_{TW} but forward scattering is becoming more preponderant for larger R_{TW}. The effect of the hole diameter on the scattering characteristics will be discussed in the next section.

IV. INFLUENCE OF DAMAGE SIZES

This section employs the experimental validated FE model to investigate the influence of the through hole size on the scattering characteristics of A_0 Lamb wave in a quasi-isotropic $[45/-45/0/90]_S$ composite laminate. A number of FE simulations using the same excitation frequency were carried out for different through hole diameters. The results are then presented in terms of R_{TW}. The range of the R_{TW} in this study is from 0.13 to 1.51 which are obtained by changing the through hole diameter while keeping the excitation frequency at 140 kHz. Fig. 7a shows the normalized amplitude calculated according to Equation (1) of the forward scattered wave as a function of R_{TW} for θ = 0°, 40°, 80°, 280° and 320°. The scatter amplitude is always largest in the forward scattering direction θ = 0° and shows an almost linear increase for increasing R_{TW} values. For θ = 40° and 320° the amplitude inceases until around R_{TW} = 1.20 after which it reduces for larger R_{TW} values. The amplitudes of θ = 80° and 280° show small variations around a trend line of small increase for increasing R_{TW} values and are always smaller than the amplitudes of θ = 0°, 40° and 320°.

Fig. 7b shows the normalized amplitudes for backward scattering angles as a function of R_{TW}. The scattered wave amplitude at θ = 140°, 180° and 220° have similar characteristics. The general trend is an increase in amplitude for increasing R_{TW} with slight variations

around these trend lines. Different to the forward scattering, the amplitudes of the backward scattering angle θ = 180° are smaller than those of θ = 140° and 220°, a phenomenon that does not exist in isotropic material. This behavior is due to the anisotropic nature of composite laminates in which the scattering energy tends to concentrate around the fiber directions of the outer two laminae. More quantitative and detailed results will be discussed in Section V. For θ = 100° and 260°, the amplitude exhibits a larger variation and slower increase with R_{TW} compared to θ = 140°, 180° and 220°. Comparing to similar analyses for delamination damage (Figs. 8a and 8b in Ng and Veidt[14]), the forward scattering amplitudes of through holes at θ = 0°, 40°, 320° have smaller magnitude. On the other hand, the backward scattering amplitudes of through holes have larger magnitude and simpler behavior comparing to delamination damage in composite laminates.

Fig. 7c shows the backward (θ = 180°) to forward (θ = 0°) scattering amplitude ratio as a function of R_{TW}. The backward scattering amplitudes are larger than the forward scattering amplitude for small R_{TW}. However, the forward scattering amplitude becomes larger when R_{TW} is larger than approximately 0.38. The trend of the backward to forward scattering amplitude ratio is reversed when R_{TW} is approximately 0.6. Beyond R_{TW} = 0.6, the amplitude ratio continues to decrease with slight variations and at a slower rate.

V. INFLUENCE OF STACKING SEQUENCE

This section investigates the effect of different stacking sequences on the A_0 Lamb wave scattering at through holes. Nine composite laminates containing eight layers of Cycom® 970/T300 unidirectional carbon/epoxy prepreg lamina but with different stacking sequences are considered. Table II shows a summary of the stacking sequences and the corresponding wavelengths at θ = 0°. Figs. 8 and 9 show the SDPs of the laminates with different stacking sequences for R_{TW} = 1.01. Fig. 8a shows the SDP of a $[0]_8$ unidirectional composite laminate. It can be seen that the scattering energy mainly concentrates around the fiber directions (θ = 0° and 180°). This shows that not only the energy of the excited Lamb wave,

but also the scattering energy mainly travels along the fiber direction. Figs. 8b and 8c show the SDP of the bidirectional composite laminates ($[0/90]_{2S}$ and $[45/-45]_{2S}$). Although the forward scattering energy (θ = 0°) still dominates, it is obvious that the scattering energy redistributes around the fiber directions.

Fig. 9 shows the SDP of quasi-isotropic composite laminates with different stacking sequences for R_{TW} = 1.0088. The stacking sequences considered are $[0/45/90/-45]_S$, $[0/90/45/-45]_S$, $[90/45/-45/0]_S$, $[90/-45/0/45]_S$, $[45/-45/0/90]_S$ and $[45/90/-45/0]_S$. It can be seen that although all six stacking sequences are quasi-isotropic with identical laminae, the SDP are quite different. An interesting observation is that the SDP of the $[0/90/45/-45]_S$ and $[45/-45/0/90]_S$ are similar to $[0/90]_{2S}$ and $[45/-45]_{2S}$, respectively. This suggests that the SDP are dominated by the fiber directions of the outer two laminae. This effect also exists for other values of R_{TW}, but the corresponding SPDs are not shown due to space limitations. This phenomenon explains the limitation of damage characterization using a diffraction tomography reconstruction methodology based on Mindlin plate theory, which the authors have reported previously[25].

Figs. 10 and 11 show the scattering amplitude as a function of both R_{TW} and θ using two-dimensional (2D) contour plot for a unidirectional, bidirectional and quasi-isotropic composite laminate, respectively. The white dash lines in Fig. 10 indicate the fiber directions of each lamina. Similar to the observation reported in Section IV, it can be seen that the forward scattering always dominates for larger R_{TW} for all considered stacking sequences (as shown in Figs. 10 and 11). In addition, the contour plots illustrate that the scattering energy is also enhanced around the fiber direction, especially for larger R_{TW}. For example, the energy is enhanced around θ = 45°, 135°, 225° and 315° for $[45/-45]_{2S}$; and around θ = 0°, 90°, 180° and 270° for $[0/90/45/-45]_S$).

Fig. 12 shows the normalized amplitude as a function of R_{TW} for θ = 0° and 180°. Basically, most of the stacking sequences have similar scattering characteristics for forward and backward scattering amplitudes but the magnitudes are different. For θ = 0°, the scattering amplitude increases almost linearly with R_{TW}. In the case of θ = 180° the

scattering amplitude shows some slight variation superimposed on a general increasing trend line. An interesting observation is that there exists a strong relation between the scattering magnitude and wavelength of the incident A_0 Lamb wave at θ = 0°. The third column of Table II shows the wavelength of the A_0 Lamb wave at 140 kHz and θ = 0°. It can be seen that the wavelength can be grouped into three categories based on the magnitude. The first group is the stacking sequence of $[0]_8$ with 9.8 mm wavelength. The second group is the stacking sequences of $[0/90]_{2S}$, $[0/45/90/-45]_S$ and $[0/90/45/-45]_S$ in which the wavelength is around 8.8 mm. The last group is the stacking sequences of $[45/-45]_{2S}$, $[90/45/-45/0]_S$, $[90/-45/0/45]_S$, $[45/-45/0/90]_S$ and $[45/90/-45/0]_S$ with wavelengths below 8 mm. Each group has its particular scattering magnitude for θ = 0° and 180° as shown in Fig. 12. This implies that the scattering magnitude depends on the wavelength of the incident A_0 Lamb wave in addition to the through hole diameter to wavelength ratio R_{TW}.

VI. CONCLUSIONS

The scattering characteristics of the A_0 Lamb wave at a through hole in composite laminates were studied in this paper. It has been demonstrated through experimental validation that 3D FE analysis is able to accurately predict Lamb wave propagation and scattering. The results of parameter studies investigating the influence of hole diameter to wavelength ratio and laminate stacking sequence on the wave scattering characteristics show that amplitude and directivity distributions of the scattered Lamb wave depend on these parameters. In the case of quasi-isotropic composite laminates, the scattering patterns are dominated by the fiber orientation of the outer layers and are quite different for composite laminates that have the same number of laminae but different stacking sequences. Both FE simulation and experimental measurements were used to gain understanding of the A_0 Lamb wave scattering characteristics. A series of parametric studies were carried out to investigate the through hole size effect on the scattered Lamb wave. The results show that the amplitude and the directivity of the scattered Lamb wave depend on R_{TW}.

The results of this study provide improved physical insight into the scattering phenomena of A_0 Lamb wave at through holes in composite laminates, which is essential to further advance the development, validation and optimization of guided wave damage detection and characterization techniques for composite materials.

ACKNOWLEDGEMENTS

C.T. Ng would like to acknowledge the financial support from the University of Queensland and Cooperative Research Centre for Advanced Composite Structures (CRC-ACS). The work has been carried out as part of the CRC-ACS research program. Computational (and/or data visualization) resources used in this work were provided by the Queensland Cyber Infrastructure Foundation. The work was also supported by the Australian Research Council under Discovery Project DP0771585.

REFERENCES

[1] N. Guo and P. Cawley, "The interaction of Lamb waves with delaminations in composite laminates" J. Acoust. Soc. Am. **94**, 2240–2246 (1993).

[2] A. Birt, "Damage detection in carbon-fibre composites using ultrasonic Lamb waves" Insight **40**, 335–339 (1998).

[3] J. L. Rose, "Guided wave nuances for ultrasonic nondestructive evaluation" IEEE Trans. Ultrason. Ferroelectr. Freq. Control **47**, 575–583 (2000).

[4] M. Lemistre and D. Balageas, "Structural health monitoring system based on diffracted Lamb wave analysis by multiresolution processing" Smart Mat. Struct. **10**, 504–511 (2001).

[5] E. V. Malyarenko and M. K. Hinders, "Fan beam and double crosshole Lamb wave tomography for mapping flaws in aging aircraft structures" J. Acoust. Soc. Am. **108**, 1631–1639 (2000).

[6] A. H. Rohde, M. Veidt, L. R. F. Rose and J. Homer, "A computer simulation study of imaging flexural inhomogeneities using plate-wave diffraction tomography," Ultrasonics, **48**, 6-15 (2008).

[7] C. T. Ng and M. Veidt, "A Lamb-wave-based technique for damage detection in composite laminates" Smart Mat. Struct. **18**, 1-12 (2009).

[8] C. Vemula and A. N. Norris, "Flexural wave propagation and scattering on thin plates using Mindlin theory" Wave Motion, **26**, 1-12 (1997).

[9] J. C. P. McKeon and M. K. Hinders, "Lamb wave scattering from a through hole" J. Sound Vib. **224**, 843-862 (1999).

[10] P. Fromme and M. B. Sayir, "Measurement of the scattering of a Lamb wave by a through hole in a plate" J. Acoust. Soc. Am. **111**, 1165-1170 (2002).

[11] F. B. Cegla, A. Rohde and M. Veidt, "Analytical prediction and experimental measurement for mode conversion and scattering of plate waves at non-symmetric circular blind holes in isotropic plates" Wave Motion **45**, 162-177 (2008).

[12] L. Moreau and M. Castaings, "The use of an orthogonality relation for reducing the size of finite element modes for 3D guided waves scattering problems" Ultrasonics **48**, 357-366 (2008).

[13] W. Ke, M. Castaings and C. Bacon, "3D finite element simulations of an air-coupled ultrasonic NDT system" NDT & E Intern. 42, 524-533 (2009)

[14] C. T. Ng and M. Veidt, "Scattering of the fundamental anti-symmetric Lamb wave at delaminations in composite laminates" Submitted to the J. Acoust. Soc. Am. (2010).

[15] K. Diamanti, C. Soutis and J. M. Hodgkinson, "Piezoelectric transducer arrangement for the inspection of large composite structures" Comp. Part A **38**, 1121-1130 (2007).

[16] P. Belanger and P. Cawley, "Feasibility of low frequency straight-ray guided wave tomography" NDT & E Int. **42**, 113-119 (2009).

[17] ANSYS 12.0, *Meshing and Modeling Guide* (ANSYS Inc., USA, 2009).

[18] LS-DYNA, *LS-DYNA Version 971 Keyword User's Manual Volume 1* (Livermore Software Technology Corporation, USA, 2007).

[19] C. C. Chamis, "Mechanics of composite materials: Past, present and future" J. Comp. Tech. Res. **11**, 3-14 (1989).

[20] D. Alleyne and P. Cawley, "The interaction of Lamb waves with defects" IEEE Trans. Ultrason. Ferroelectr. Freq. Control **39**, 381-397 (1992).

[21] M. J. S. Lowe, P. Cawley, J. Y. Kao and O. Diligent "The low frequency reflection characteristics of the fundamental antisymmetric Lamb wave ao from a rectangular notch in a plate" J. Acoust. Soc. Am. **112**, 2612-2622 (2002).

[22] J. R. Stewart, A. S. Gullerud and M. W. Heinstein, "Solution verification for explicit transient dynamics problems in the presence of hourglass and contact forces." Comp. Meth. in App. Mech. and Eng. **195**, 1499-1516 (2006).

[23] B. Pavlakovic and M. J. S. Lowe, *DISPERSE: A System for Generating Dispersion Curves, User's Manual Version 2.0.16B* (Imperial College, University of London, London, 2003).

[24] K. Kishimoto, H. Inoue, M. Hamada and T. Shibuya, "Time frequency analysis of dispersive waves by means of wavelet transform" J. Appl. Mech. 62, 841-848 (1995).

[25] C. T. Ng, M. Veidt and N. Rajic. "Integrated piezoceramic transducers for imaging damage in composite laminates" Proceeding of SPIE **7493**, 1-8 (2009).

[26] L. Wang and F. G. Yuan, "Group velocity and characteristic wave curves of Lamb waves in composites: modeling and experiments" Comp. Sci. Tech. **67**, 1370-1384 (2007).

[27] C. Potel, S. Baly, J. F. de Belleval, M. J. S. Lowe and P. Gatignal, "Deviation of monochromatic lamb wave beam in anisotropic multilayered media: asymptotic analysis, numerical and experimental results" IEEE Trans. Ultrason. Ferroelectr. Freq. Control **52**, 987-1001 (2005).

[28] K. Balasubramaniam and C. V. Krishnamurthy, "Ultrasonic guided wave energy behavior in laminated anisotropic plates" J. Sound Vib. **296**, 968-978 (2006).

TABLE I: Effective material properties of Cycom® 970/T300 prepreg lamina

E_{11} (GPa)	E_{22} (GPa)	E_{33} (GPa)	G_{12} (GPa)	G_{13} (GPa)	G_{23} (GPa)	ν_{12}	ν_{13}	ν_{23}	ρ (kg/m^3)
128.75	8.35	8.35	4.47	4.47	2.90	0.33	0.33	0.44	1517

TABLE II: Summary of composite laminates with different stacking sequences

Composite laminate	**Stacking sequence**	**Wavelength for θ = 0° and 140 kHz (mm)**
Unidirectional	$[0]_8$	9.80
Bidirectional	$[0/90]_{2S}$	8.83
Bidirectional	$[45/-45]_{2S}$	7.85
Quasi-isotropic	$[0/45/90/-45]_S$	8.80
Quasi-isotropic	$[0/90/45/-45]_S$	8.80
Quasi-isotropic	$[90/45/-45/0]_S$	7.17
Quasi-isotropic	$[90/-45/0/45]_S$	7.22
Quasi-isotropic	$[45/-45/0/90]_S$	7.93
Quasi-isotropic	$[45/90/-45/0]_S$	7.60

FIGURE CAPTIONS

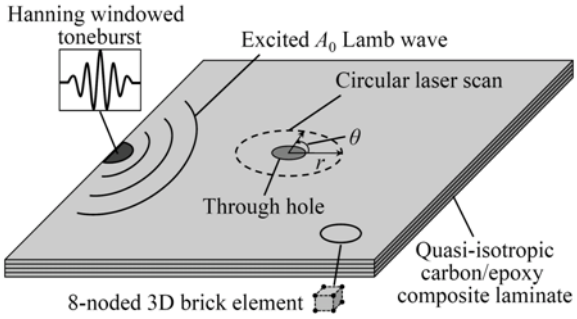

FIG. 1 Schematic diagram of the configuration for FE simulations

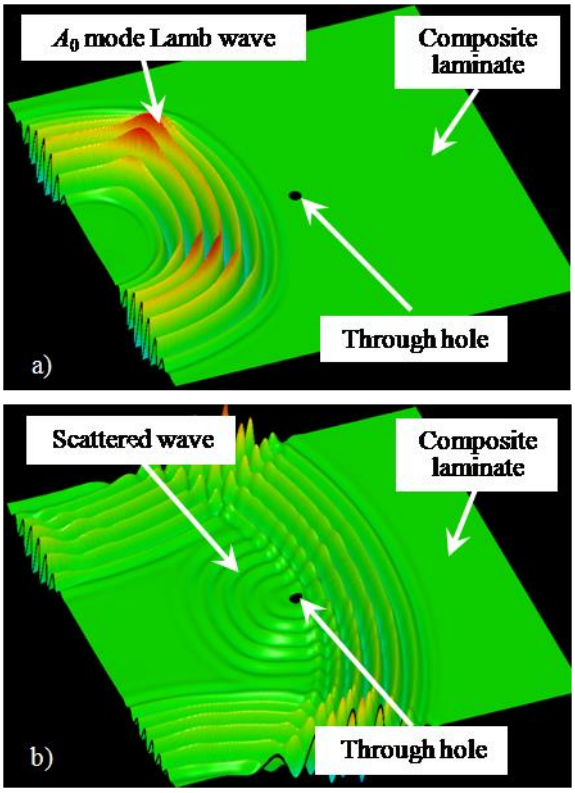

FIG. 2 Typical contour snapshots of FE simulated out-of-plane displacement for the $[45/-45/0/90]_S$ composite laminate, a) soon after excitation and b) scattered wave from a through hole damage

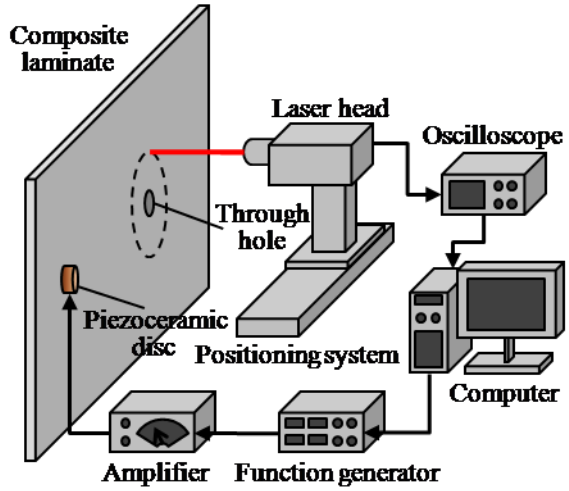

FIG. 3 Schematic diagram of the experimental set-up

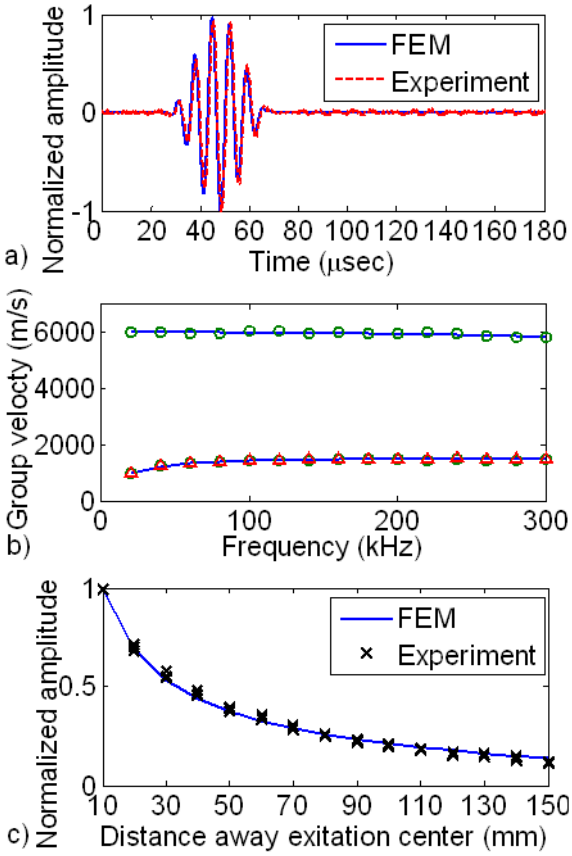

FIG. 4 a) Normalized incident Lamb wave at location $r = 40$ mm and $\theta = 0°$, b) group velocity dispersion curve at $\theta = 0°$, and c) normalized out-of-plane displacement amplitude as a function of wave propagation distance at $\theta = 0°$ in the $[45/-45/0/90]_S$ composite laminate

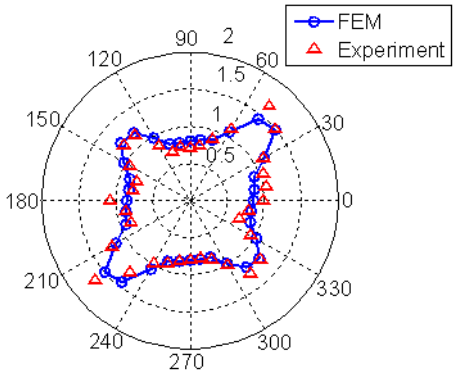

FIG. 5 Normalized polar directivity excitation amplitude of the $[45/-45/0/90]_S$ composite laminate at r = 40 mm from transducer

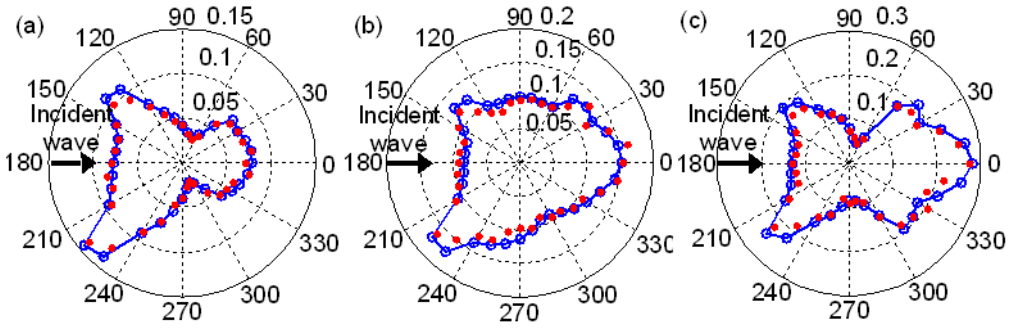

FIG. 6 Scattering directivity pattern for a) 3 mm, b) 5 mm and c) 8 mm diameter circular through hole damage in a $[45/-45/0/90]_S$ composite laminate by 140 kHz incident wave (FE simulation: line with empty circles, experiment: filled circles)

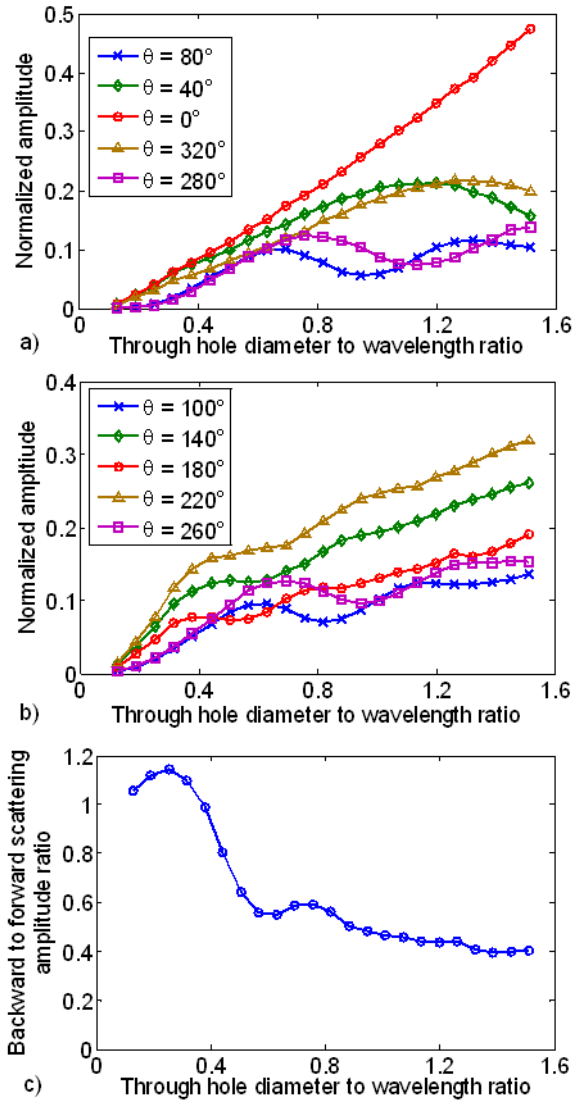

FIG. 7 Normalized amplitude for a) forward scattering, b) backward scattering and c) backward to forward scattering ratio as a function of the through hole diameter to the wavelength ratio in the $[45/-45/0/90]_S$ composite laminate

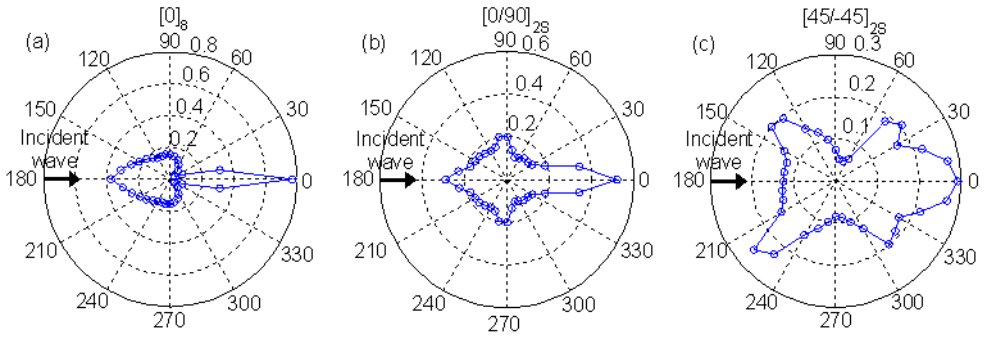

FIG. 8 Scattering directivity pattern of the $[0]_8$, $[0/90]_{2S}$ and $[45/-45]_{2S}$ composite laminates for R_{TW} = 1.0088

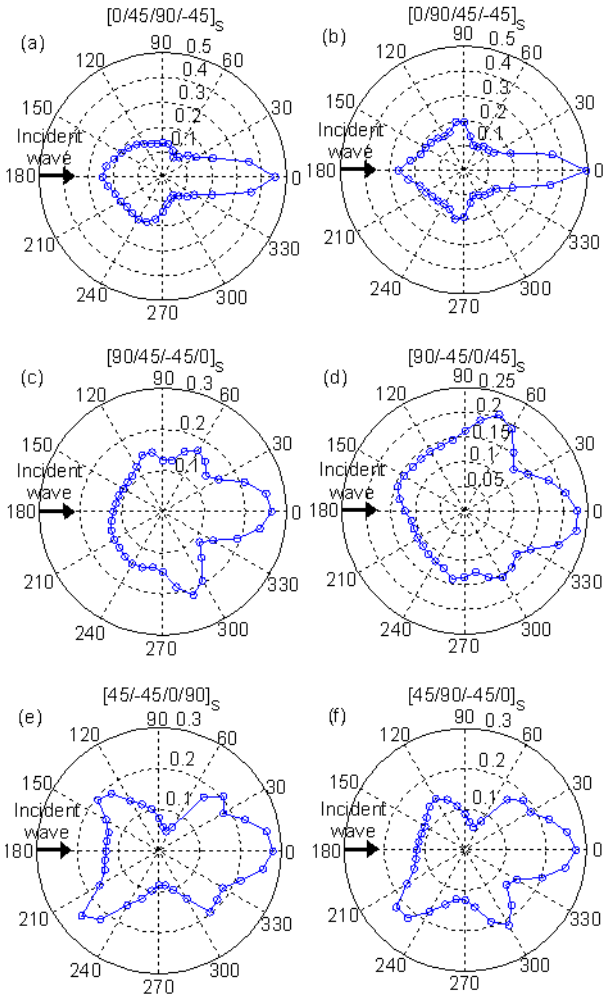

FIG. 9 Scattering directivity pattern of the $[0/45/90/-45]_S$, $[0/90/45/-45]_S$, $[90/45/-45/0]_S$, $[90/-45/0/45]_S$, $[45/-45/0/90]_S$ and $[45/90/-45/0]_S$ composite laminates for R_{TW} = 1.0088

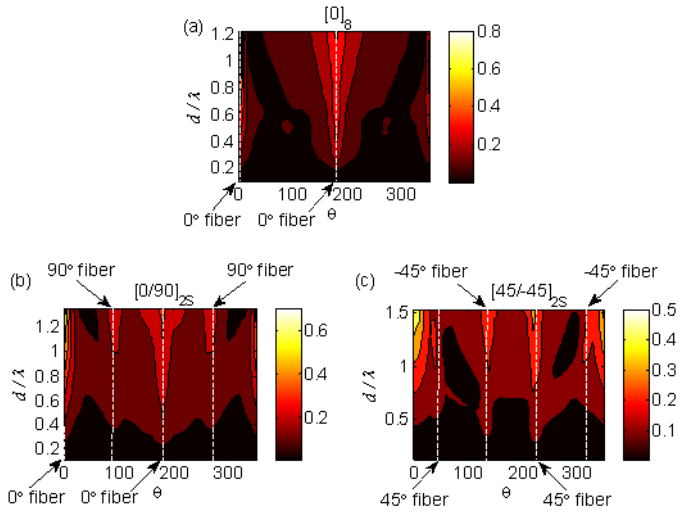

FIG. 10 Contour plot of normalized amplitude as a function of R_{TW} and θ for the $[0]_8$, $[0/90]_{2S}$ and $[45/-45]_{2S}$ composite laminates

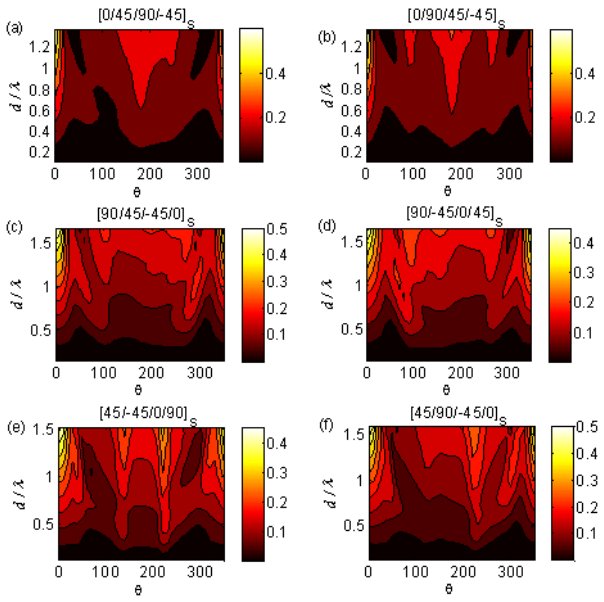

FIG. 11 Contour plot of normalized amplitude as a function of R_{TW} and θ for the $[0/45/90/-45]_S$, $[0/90/45/-45]_S$, $[90/45/-45/0]_S$, $[90/-45/0/45]_S$, $[45/-45/0/90]_S$ and $[45/90/-45/0]_S$ composite laminates

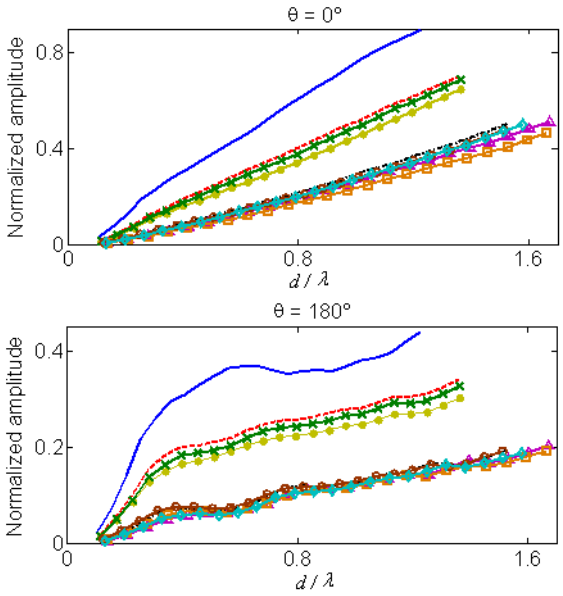

FIG. 12 Normalized amplitude as a function of R_{TW} for θ = 0 and 180°(solid line: $[0]_8$, dash line: $[0/90]_{2S}$, dash-dot line: $[45/-45]_{2S}$, filled circles: $[0/45/90/-45]_S$, crosses: $[0/90/45/-45]_S$, triangles: $[90/45/-45/0]_S$, squares: $[90/-45/0/45]_S$, circles: $[45/-45/0/90]_S$, rhombus: $[45/90/-45/0]_S$)